DOI: 10.1002/ejic.200601135

Oriented Attachment Growth of Three-Dimensionally Packed Trigonal Selenium Microspheres into Large-Area Wire Networks

Liangbao Yang,[a] Yuhua Shen,*[a] Anjian Xie,[a] and Jianjun Liang[b]

Keywords: Nanostructures / Self-assembly / Selenium

The formation of Se microwire networks by hydrothermal treatment in tungstosilicic acid solution is described. The kinetics of crystallization of the Se assembly is studied as a function of reaction time. During the formation process, single-crystal Se rods can direct the self-aggregation of the amorphous nanoparticles derived from a supersaturation precipitation reaction and promote their crystallization and transformation under mild hydrothermal conditions. In this system, the rod-directed epitaxial aggregation of Se was clearly observed in addition to the traditional Ostwald ripening process.

Introduction

Solution synthesis has been an important route to nanoparticles with specific shape, size, orientation, etc., which play key roles in tailoring the properties of nanomaterials. Traditional solution-synthetic methods have been widely used for the controlled synthesis of various colloidal nanoparticles.[1] There are different opinions on the mechanisms of morphological synthesis of inorganic nanoparticles. One basic crystal-growth mechanism in solution systems is the well-known "Ostwald ripening process".[2] In the Ostwald ripening process, the formation of tiny crystalline nuclei in a supersaturated medium occurs first. This is followed by crystal growth, in which the larger particles will grow at the cost of the smaller ones, because the smaller ones have a higher solubility on the basis of the Gibbs–Thompson law.[3] Another growth mechanism mainly involving oriented particle aggregation,[4–7] which was conceptually termed "oriented attachment" by Penn and Banfield et al.,[8–12] has emerged recently.[13] In this theory, the bigger particles grow from small primary nanoparticles through an orientated attachment process in which the adjacent nanoparticles self-assemble by sharing a common crystallographic orientation and by docking themselves at a planar interface.[9]

More and more evidence has been observed in several systems for either directed or undirected particle aggregation. A growth mode of this kind can lead to the formation of faceted particles or anisotropic growth if it occurs near equilibrium and if there is sufficient difference in the surface energies of different crystallographic faces.[11] Very recently, Shu-Hong Yu et al. reported evidence for the oriented attachment mechanism in which the nanorods obviously act as epitaxial "substrates" or guide the directional aggregation process for the formation of nanorod-based aggregated structures.[14]

Tungstosilicic acid ($H_4SiW_{12}O_{40}$, TSA) ions form a subset of the polyoxometalates that have Keggin structure. Polyoxometalates with Keggin structure have the general formula $(XM_{12}O_{40})^{(8-n)-}$, where "M" stands for the element W or Mo, "X" stands for heteroatoms such as P, Si, Ge, and n is the valency of X.[15] It is well known that Keggin ions undergo stepwise multielectron redox processes without structural change.[15] They may be reduced electrolytically, photochemically, and chemically (with suitable reducing agents). They are a large category of metal–oxygen cluster anions with well-defined structures and properties, with diverse applications in the fields of analytical chemistry, biochemistry, and solid-state devices, and have been used as antiviral and antitumor reagents. Their redox chemistry is characterized by their ability to accept and release a certain number of electrons, in distinct steps, without decomposition.[16]

Selenium is a material suitable for a self-organization studies, because of the excellent ability of trigonal selenium (t-Se) to grow preferentially along the *c* axis and the possibility of controlling the one-dimensional growth of selenium by diverse approaches.[17–21] If its three-dimensionally packed precursor is obtained, it is possible to transform it to a crossed nanowire array by choosing proper experimental conditions. Due to its photoconductivity with a spectral sensitivity that covers almost the entire visible range, selenium is also important in a wide variety of applications that

[a] School of Chemistry and Chemical Engineering, Anhui University,
Hefei 230039, P. R. China
Fax: +86-551-5107342
E-mail: s_yuhua@163.com
[b] Chuzhou Vocational Technology College,
Chuzhou 239000, P. R. China

Supporting information for this article is available on the WWW under http://www.eurjic.org or from the author.

range from photocells, photographic exposure meters, and solar cells to semiconductor rectifiers. In this study, we have designed a hydrothermal synthesis for the selenium microcrystal. To the best of our knowledge, a hydrothermal synthesis of a Se single crystal with this novel structure has not been achieved previously in TSA solution.

Results and Discussion

Figure 1A presents the Raman spectrum of the synthesized sample. The resonance peak at 233 cm^{-1} is a characteristic signature of trigonal selenium, which can be assigned to the vibration of the Se helical chain.[14] A peak around 142 cm^{-1} results from the transverse optical photon mode. For comparison, the characteristic Raman peaks for monoclinic selenium and α-Se are at 256 cm^{-1} and 264 cm^{-1}, respectively.[22] The XRD pattern recorded from a drop-coated film of the sample on a glass substrate is shown in Figure 1B, curve a. All of the strong and sharp reflection peaks can be readily indexed to a single phase of trigonal-structured selenium [t-Se, space group $P3_121$ (152)] containing infinite, helical chains of selenium atoms packed parallel to each other along the *c* axis, with cell parameters $a = 0.4367$ nm and $c = 0.4959$ nm. These values are in agreement with the values reported in the literature.[23] For comparison, the XRD spectrum of bulk t-Se is shown in Figure 1B, curve b; it is similar to the spectra recorded by the Xie group.[24,25] These results, obtained from Raman spectroscopy and XRD, indicate that the product is crystalline.

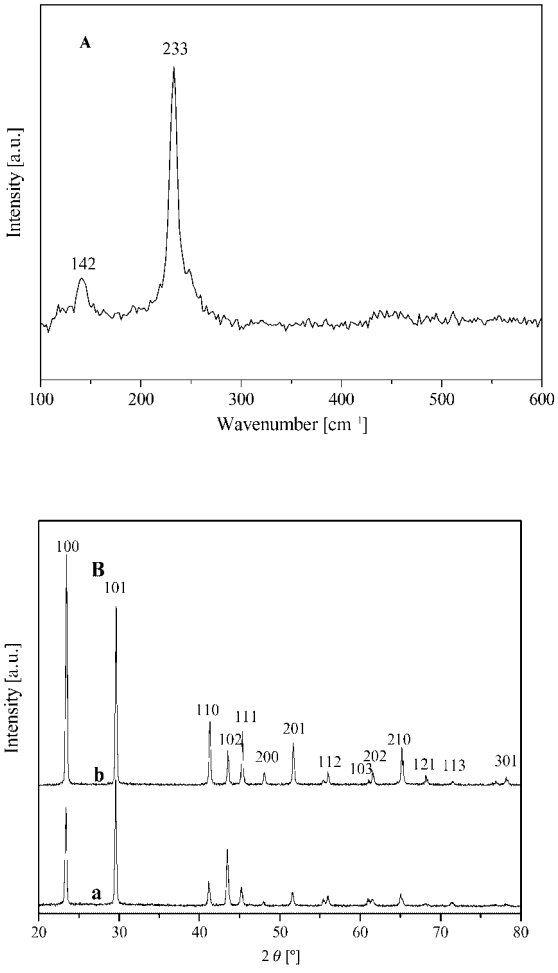

Figure 1. Raman spectrum of the synthesized sample (A) and XRD pattern (B) of a sample of the precipitates obtained as a result of hydrothermal treatment (curve a) and a sample of the bulk t-Se (curve b).

The product was characterized by using scanning electron microscopy (SEM), and a typical image is shown in Figure 2. The image shown in Figure 2A clearly reveals that a large-area microwire network was successfully fabricated. The units for the build-up of the network are uniform microwires with an average diameter of about 1.5 μm and lengths of up to hundreds of micrometers. The aspect ratio of the wire is in the range of several hundreds, which may be a useful feature in some applications. The structure and morphology of the microwires was further characterized by transmission electron microscopy (TEM) and selected-area electron diffraction (SAED). Figure 2B shows a typical TEM image of the microwires, revealing their high aspect ratio, good crystallinity, and uniformity. Figure 2C shows

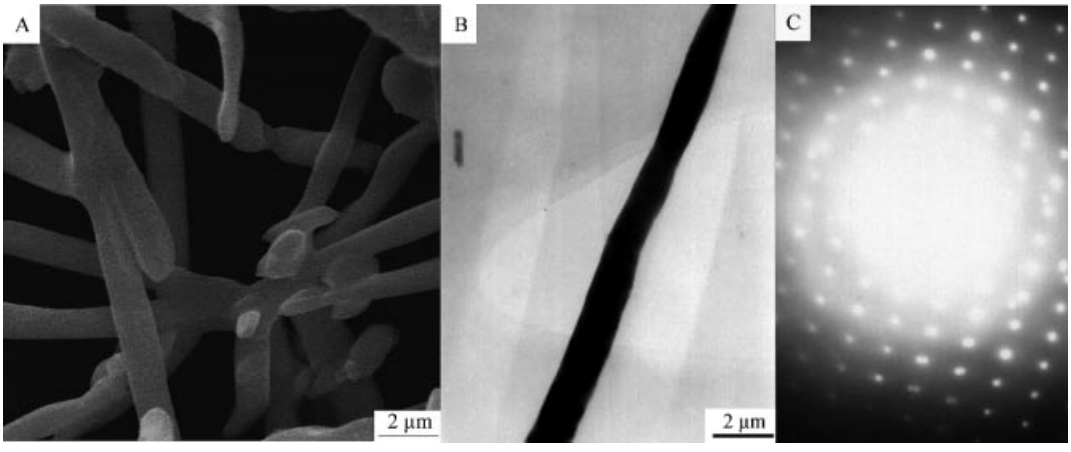

Figure 2. A representative SEM image (A), the TEM image (B), and the associated SAED pattern of the t-Se microcrystal (C).

the associated SEAD pattern recorded by focusing the incident electron beam on an individual microwire and exhibits the single-crystalline nature of the wire. The twofold rotational symmetry associated with this pattern indicates that these t-Se wires have predominately grown along the [001] direction (*c* axis), with the helical *c* chains of the Se atoms parallel to the longitudinal axis.[26] We have also carried out extensive investigations on more individual wires by using electron diffraction (ED), the results of which demonstrate that the as-synthesized sample is single-crystalline.[26]

To ensure that the TSA present in the system has an important effect on the synthesis of the Se particles, a control experiment was performed under the the same conditions, but only without TSA. A lot of irregular microparticles were obtained (see the SEM image in the Supporting Information, FigureS1). On the basis of the above analyses, we conclude that TSA significantly affects the shapes of the particles.

To study the formation mechanism of the network of t-Se microwires, various growth stages of the t-Se microwire network were investigated. Figure 3 shows a set of SEM images corresponding to samples obtained at different growth stages of the microwire. After 1 h of hydrothermal treatment, spherical α-Se was obtained (Figure 3A), and no ED pattern was detected. The image shows highly uniform colloidal particles of predominantly spherical morphology. An analysis of 100 such particles from several SEM micrographs resulted in determination of the average particle size of 64 ± 14 nm. When the solution was treated for 3 h, spherical t-Se particles were formed, and some of the spheres were broken (Figure 3B). The size of t-Se spherical particles was about 3.5 ± 1.4 μm. In Figure 3C, it is clearly seen that most of the spheres are broken, and an interesting core–shell structure is revealed. The structural characteristics of the crystal were further elucidated by the TEM and ED techniques (inset in Figure 3C). The SAED patterns for the shell and core areas are identical. A further investigation of such a complex growth process is ongoing. The Se rods formed at the initial stage from the seeds of spherical t-Se were observed at a hydrothermal treatment time of 6 h (Figure 3D). It can be seen that some rods and a lot of spheres coexist. The Se microrods grew as the hydrothermal treatment time was prolonged to 12 h. The number of rods increased, the rods became longer, and the spheres tailed off. Most of the spheres grew alongside the rods (Figure 3E). After 24 h of treatment, the t-Se microwires grew into a well-organized, shaped network (Figure 3F), and any longer treatment made no difference in the morphology.

According to the Stranski rule, in crystals that may exhibit various allotropes, the least stable and most soluble phase, which is favored kinetically, usually precipitates first, and then this metastable phase is transformed during the aging process into a more thermodynamically stable phase.[27] In order to understand the growth process of the Se microwires on the basis of the results obtained, a feasible route is presented as shown in Figure 4. First, the unstable spherical α-Se particles are formed (a). Second, α-Se transforms into the more stable t-Se. Under hydrothermal treatment, the Se rods begin to grow on the surface of the spherical t-Se (c–f); then the Se microrods are formed after continuous growth, and at last, the microrods are transformed into the microwire network by the Ostwald ripening process (g). We believe that the aggregated growth along the circumference of the gap in the broken sphere resulting from the hydrothermal treatment leads to the formation of microrods, which is similar to the conclusion reached by Yang et al.[28] It seems that the situation is almost the same in this study. The long-term hydrothermal treatment somehow breaks the selenium sphere and forms a crater on the sphere. The edge of the crater acts as the initiation spot, and further directional growth of the selenium crystal along this crater yields the rod product. The transition of microrods into the microwire network indicates that the wires are thermodynamically stable.

The conventional hydrothermal crystallization or transformation process with amorphous nanoparticles as precursors is a typical Ostwald ripening process, in which a highly supersaturated solution is adopted, and amorphous fine particulates act as the precursors. In this mechanism, the formation of tiny crystalline nuclei in a supersaturated medium occurs at first and is then followed by crystal growth. The larger particles (Figure 3B) will grow at the expense of the small ones (Figure 3A) because of the difference in solubility between large and smaller particles according to the well-known Gibbs–Thomson law. In the early stage, the examination of intermediate products (Figure 3D) shows the coexistence of the short rods and microspherical particles. As the reaction goes on, the microspheres decrease in number, and longer microrods form (Figure 3E), suggesting that the longer rods obviously grow at the expense of the microspheres. On the other hand, we think that the growth mode for rods in our work is similar to the seed-mediated growth mechanism of metals.[29–31] The so-called rod-directed self-aggregation process in our case is the directional aggregation of the tiny spherelike particles on the backbone of the rods. Crystalline microrods with rough surface structures then transform into the microwire network.

We performed an additional experiment to determine whether the growth process was a "ripening" or an "oriented attachment". A fresh mixture of H_2SeO_3 and TSA was added to the solutions in the presence of a suitable amount of single-crystal Se wires (0.1 mmol), and the mixture was heated at 160 °C for 3 h. The pure Se wire networks with a typical shape are shown in Figure 5. In general, Se nanospheres transform into networks in 24 h. In this experiment, this process only needed 3 h. The results indicated that all small particles tend to attach onto the backbone of the nanowires and then form micronetworks. It is interesting that no individual dispersed nanoparticles were found in the solution.

A control experiment was performed wherein microspheres were autoclaved for 12 h at 160 °C. At first, the wires and the spheres coexisted (Figure 6A), and then the wire networks were formed (shown in Figure 6B). There is little difference in morphology between Figure 6B and Fig-

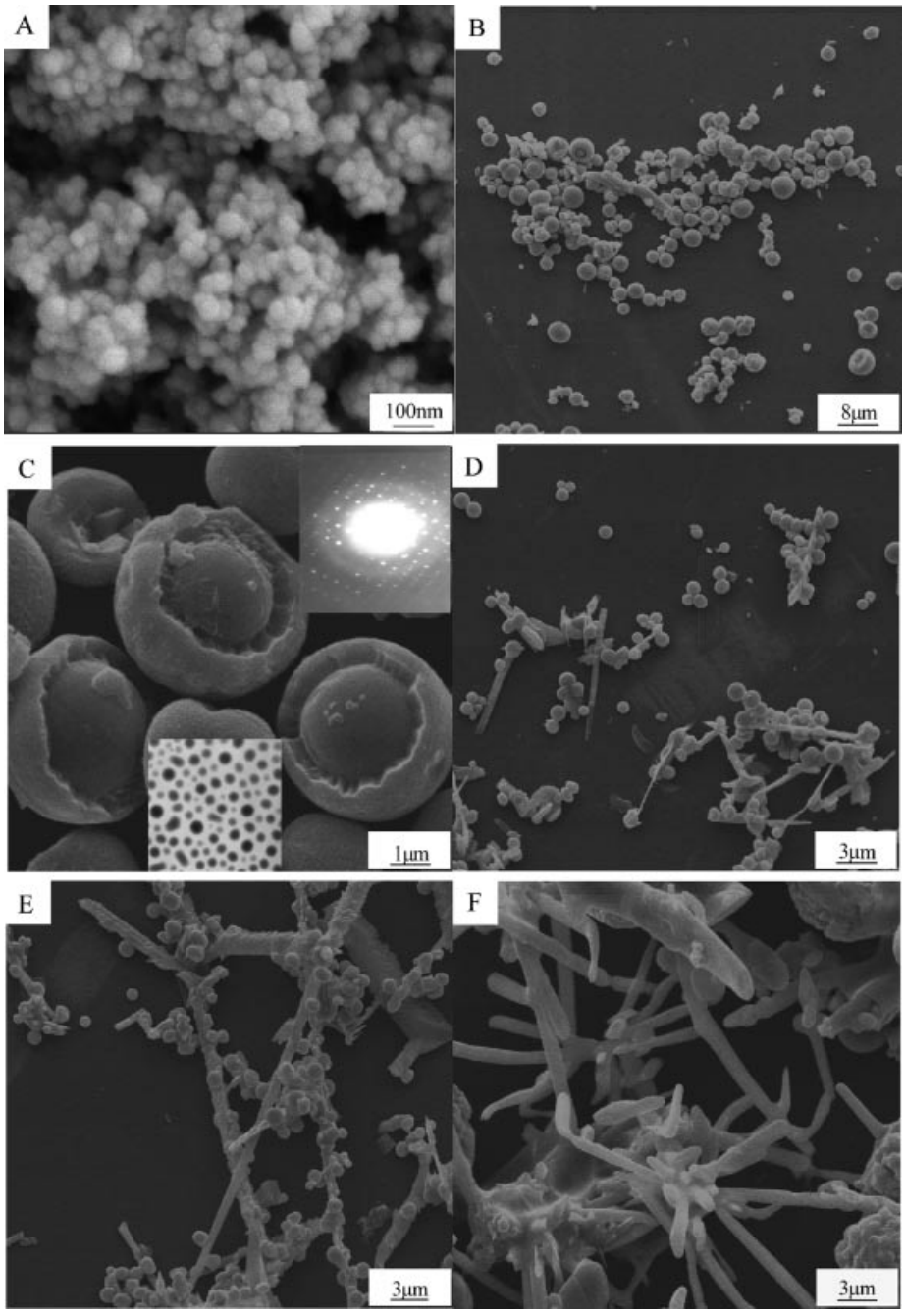

Figure 3. A set of SEM images corresponding to samples at different stages of growth of the microwire network obtained by hydrothermal treatment: after 1 h (A); low (B) and high magnifications of the rough microspheres after 3 h (C), 6 h (D), 12 h (E), and 24 h (F). The insets of (C) are the TEM and ED patterns.

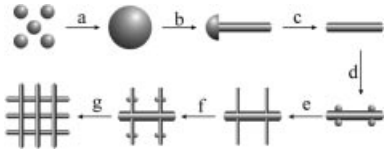

Figure 4. Formation of the wire networks by hydrothermal crystallization. In the early stage, there are a plenty of spheres (a,b); later the short rods and small nanospheres coexist (c–f); at last, the networks of Se form (g).

ure 5. These results indicated that the obvious Se-wire-directed oriented attachment mechanism and its promotion of further crystallization and transformation of the nanoparticulates are undoubtedly the mechanisms involved.

Such spontaneous "landing" of the small spherical particles on the backbone of the rods (Figure 3E) followed by the self-aggregation of these combinations of spheres and rods instead of aggregation among the small particles only could be related with one mechanism: the so-called "contact epitaxy" proposed by Averback et al.[32,33] The driving

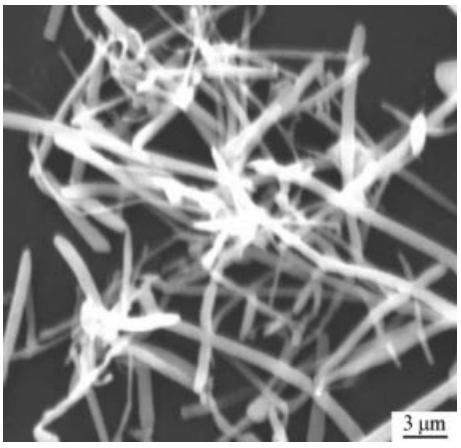

Figure 5. Typical SEM image of the sample which was obtained after adding a fresh mixture of H_2SeO_3 and TSA solutions to a 20-mL solution containing 0.1-mmol Se wires and heating the mixture for 3 hours.

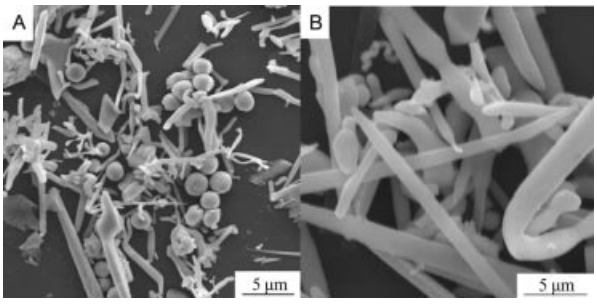

Figure 6. Typical SEM images of the samples which were obtained after heating the microspheres in an autoclave for 2 h (A) and 12 h (B).

force for this spontaneous oriented attachment is that the elimination of the pairs of high energy surfaces will lead to a substantial reduction in the surface free energy from the thermodynamic viewpoint.[10,13] The initial randomly oriented crystals can align epitaxially with the substrate (which are the rods here). This alignment is explained as the rotation of the particles within the aggregates driven by short-range interactions between adjacent surfaces.[32,33]

The surfactants were found to significantly affect the shape of the particles. The shape of the particles obtained in the presence of surfactants was completely different from that observed without surfactants. The surfactant (CTAB or SDB) plays an important role in controlling the mor-

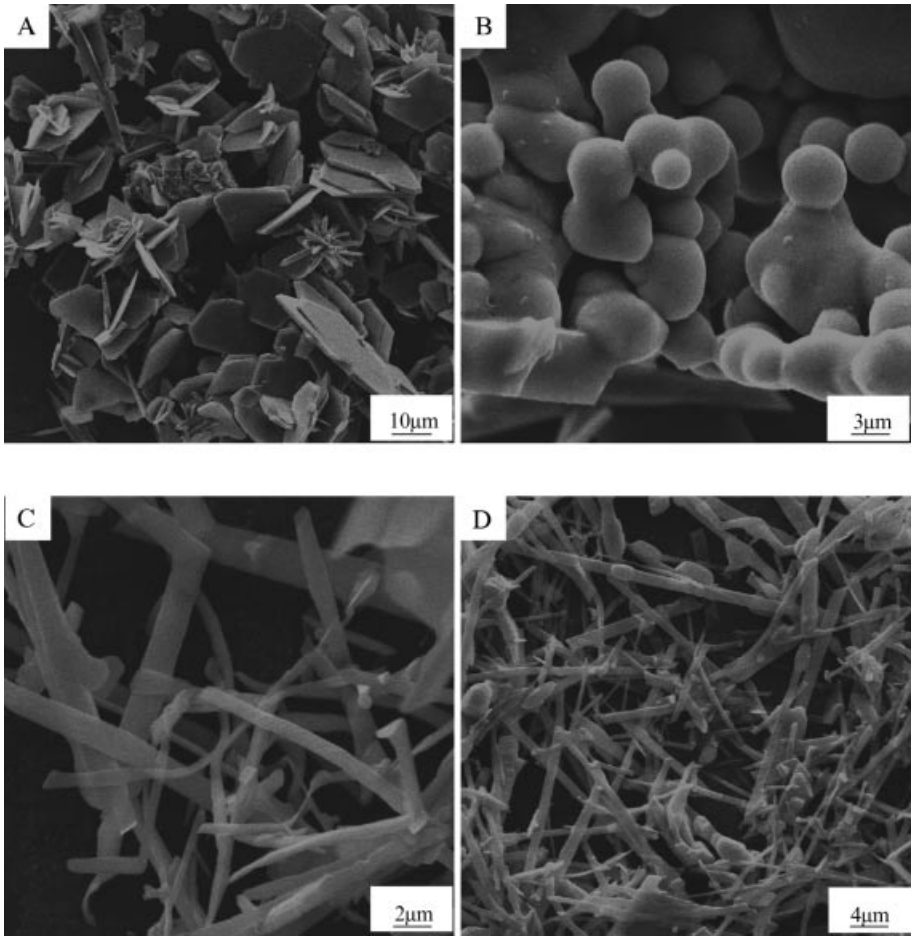

Figure 7. The SEM images of the Se particles synthesized by hydrothermal treatment for 6 h in the presence of CTAB/SDB: CTAB 0.1 M (A); CTAB 0.01 M (B); SDB 0.1 M (C); SDB 0.01 M (D).

phology of Se. When the other conditions are kept the same but CTAB (0.1 M) is added, plenty of flakes are obtained (Figure 7A). When the concentration of CTAB decreases to 0.01 M, there is some effect on the morphology of the Se crystals (Figure 7B). When SDB is added instead of CTAB, a lot of microrods and microbands are obtained at higher concentrations (Figure 7C, 0.1 M) and at lower concentrations (Figure 7D, 0.01 M). This observation can be explained by the fact that CTAB or SDB is adsorbed on specific facets of the Se crystal and changes the surface energy if the amount of CTAB or SDB is appropriate. In contrast, the nonadsorbed facets will grow rapidly. This behavior is similar to that observed in the synthesis of other crystals controlled by a surfactant.[34] When the concentration of CTAB is too low, there will not be enough surfactant adsorbed on all of the facets, and the surfactant loses the ability to control the morphology of the growing crystals (see Figure 7B).

Conclusion

In summary, on the basis of the structure and surface analysis data, we conclude that the formation of wire networks in our work is based on the Ostwald ripening process and the oriented attachment mechanism. Such spontaneous self-aggregation and crystallization induced by the well-crystallized rods could provide a unique route for improving the properties of an anisotropic material. We believe that this finding could be extended to various oxide systems or even to non-oxide rod systems.

Experimental Section

Chemicals: TSA, selenious acid (H_2SeO_3), propan-2-ol [$CH_3CH(OH)CH_3$], cetyltrimethylammonium bromide (CTAB), and sodium dodecyl sulfonate (SDS), were all A.R. grade and obtained from Shanghai Reagent Co. All the reagents in the experiments were used as received. Double-distilled water was used to prepare the solutions.

Preparation of Se Nanoparticles: In a typical experiment, an aqueous deaerated solution of TSA (30 mL, 1 mM) was taken in a test tube along with an aqueous deaerated solution of H_2SeO_3 (30 mL, 1 mM) and propan-2-ol (2 mL). About 20 mL of the solution was transferred into a 25-mL stainless-steel, Teflon-lined autoclave. The autoclave was sealed, maintained at 160 °C for the corresponding time, and then cooled to room temperature naturally. The precipitates obtained were centrifuged, washed several times with distilled water and absolute ethanol, and dried in vacuo at 60 °C for 6 h. The procedure of the corresponding control experiments with addition of different surfactants to the reaction solution is similar to the above experiments.

Analysis: FTIR spectroscopy measurements were carried out with a Nexus 870 FTIR spectrophotometer having a resolution of 4 cm^{-1} (America Nicolet Co.). SEM measurements were performed with a Leica Stereoscan-440 scanning electron microscope. The Raman spectra were recorded with a Jobin Yvon HR800 (Horiba group) instrument by using 514.5 nm as the excitation line. The products were characterized by their X-ray diffraction (XRD) patterns, which were recorded with an MXP 18 AHF X-ray diffractometer (MAC Science Co. Ltd.) with monochromatized Cu-K_α radiation (λ = 1.54056 Å). XPS measurements of Se nanoparticles were carried out with a VG ESCALAB MKII instrument at a pressure less than 10^{-6} Pa. The general scan and Se core-level spectra were recorded with non-monochromatized Mg-K_α radiation (photon energy = 1253.6 eV). The core-level binding energies (BEs) were aligned with respect to the C_{1s} binding energy (BE) of 285 eV. Samples for TEM analysis were prepared by drop-coating films of the Se solution on carbon-coated copper TEM grids, allowing the grid to stand for 2 min, and then removing the extra solution with blotting paper. The TEM measurements mentioned above were carried out with a JEM model 100SX electron microscope (Japan Electron Co.) operated at an accelerating voltage of 80 kV.

Supporting Information (see footnote on the first page of this article): SEM image of the Se particles synthesized without TSA.

Acknowledgments

This work is supported by the National Science Foundation of China (20471001, 20371001), the Specific Project for Talents of Science and Technology of Universities of Anhui Province (2005hbz03), the Key Laboratory of Environment-Friendly Polymer Materials of Anhui Province, and Science Foundation of Anhui Province (2006KJ155B).

[1] E. Matijevic, *Curr. Opin. Colloid Interface Sci.* **1996**, *1*, 176–183.
[2] T. Sugimoto, *Adv. Colloid Interface Sci.* **1987**, *28*, 65–108.
[3] J. W. Mullin, *Crystallization*, 3rd ed., Butterworth-Heinemann, Oxford, **1997**.
[4] J. K. Bailey, C. J. Brinker, M. L. Mecartney, *J. Colloid Interface Sci.* **1993**, *157*, 1–13.
[5] M. Ocana, M. P. Morales, C. J. Serna, *J. Colloid Interface Sci.* **1995**, *171*, 85–91.
[6] V. Privman, D. V. Goia, J. Park, E. Matijevic, *J. Colloid Interface Sci.* **1999**, *213*, 36–45.
[7] A. Chemseddine, T. Moritz, *Eur. J. Inorg. Chem.* **1999**, 235–245.
[8] R. L. Penn, J. F. Banfield, *Geochim. Cosmochim. Acta* **1999**, *63*, 1549–1557.
[9] R. L. Penn, J. F. Banfield, *Science* **1998**, *281*, 969–971.
[10] F. Banfield, S. A. Welch, H. Zhang, T. T. Ebert, R. L. Penn, *Science* **2000**, *289*, 751–754.
[11] R. L. Penn, G. Oskam, T. J. Strathmann, P. C. Searson, A. T. Stone, D. R. Veblen, *J. Phys. Chem. B* **2001**, *105*, 2177–2182.
[12] R. L. Penn, A. T. Stone, D. R. Veblen, *J. Phys. Chem. B* **2001**, *105*, 4690–4697.
[13] A. P. Alivisatos, *Science* **2000**, *289*, 736–737.
[14] B. Liu, S.-H. Yu, F. Zhang, L. J. Li, Q. Zhang, L. Ren, K. Jiang, *J. Phys. Chem. B* **2004**, *108*, 2788–2792.
[15] a) M. T. Pope, A. Muller, *Angew. Chem. Int. Ed. Engl.* **1991**, *30*, 34–48; b) V. Kogan, Z. Izenshtat, R. Neumann, *Angew. Chem. Int. Ed.* **1999**, *38*, 3331–3334.
[16] M. T. Pope in *Inorganic Chemistry Concepts* (Eds.: C. K. Jorgensen, M. F. Lappert, S. J. Lippard, J. L. Margrave, K. Niedenzu, H. Nobh, R. W. Parry, H. Yamatera), Springer Verlag, West Berlin, **1983**, vol. 8, p. 101.
[17] B. Gates, Y. Yin, Y. Xia, *J. Am. Chem. Soc.* **2000**, *122*, 12582–12583.
[18] B. Gates, B. Mayers, A. Grossman, Y. Xia, *Adv. Mater.* **2002**, *14*, 1749–1752.
[19] X. Zhang, Y. Xie, F. Xu, X. H. Liu, *Chin. J. Inorg. Chem.* **2003**, *19*, 77–81.
[20] Y. Ding, Q. Li, Y. B. Jia, L. Chen, J. Y. Xing, Y. T. Qian, *J. Cryst. Growth* **2002**, *241*, 489–497.

[21] A. Abdelousa, W. L. Gong, W. Lutze, J. A. Shelnutt, R. Franco, J. Moura, *Chem. Mater.* **2000**, *12*, 1250–1256.
[22] B. Gates, B. Mayers, B. Cattle, Y. Xia, *Adv. Funct. Mater.* **2002**, *12*, 219–227.
[23] C. H. An, K. B. Tang, X. M. Liu, Y. T. Qian, *Eur. J. Inorg. Chem.* **2003**, 3250–3255.
[24] B. Zhang, X. Ye, Y. Xie, *Nanotechnology* **2006**, *17*, 385–390.
[25] X. B. Cao, Y. Xie, L. Y. Li, *Adv. Mater.* **2003**, *15*, 1914–1918.
[26] L. Stuke in *Selenium* (Eds: R. A.Zingaro, W. C. Cooper), van Nostrand Reinhold, New York, **1994**.
[27] J. P. Jolivet, M. Henry, J. Livage, *Metal Oxide Chemistry and Synthesis - from Solution to Solid State*, John Wiley and Sons, Chichester, U. K. **2000**, p. 47.
[28] H. Zhang, D. Yang, Y. Ji, X. Ma, D. Que, *J. Phys. Chem. B* **2004**, *108*, 1179–1182.
[29] H. Liao, J. H. Hafner, *J. Phys. Chem. B* **2004**, *108*, 19276–19280.
[30] a) Z. Wei, A. J. Mieszawska, F. P. Zamborini, *Langmuir* **2004**, *20*, 4322–4326; b) Z. Wei, F. P. Zamborini, *Langmuir* **2004**, *20*, 11301–11304.
[31] N. Taub, O. Krichevski, G. Markovich, *J. Phys. Chem. B* **2003**, *107*, 11579–11582.
[32] H. L. Zhu, R. S. Averback, *Philos. Mag. Lett.* **1996**, *73*, 27–33.
[33] M. Yeadon, M. Ghaly, J. C. Yang, R. S. Averback, J. M. Gibson, *Appl. Phys. Lett.* **1998**, *73*, 3208–3210.
[34] Y. W. Jun, M. F. Casula, J. H. Sim, S. Y. Kim, J. Cheon, A. P. Alivisatos, *J. Am. Chem. Soc.* **2003**, *125*, 15981–15985.

Received: November 30, 2006
Published Online: August 9, 2007

